ISSN: 2447-3359

REVISTA DE GEOCIÊNCIAS DO NORDESTE

Northeast Geosciences Journal

v. 11, nº 2 (2025)

https://doi.org/10.21680/2447-3359.2025v11n2ID40616

Application of The Ransac Method to Stabilize the Camera Referential In High-Precision Inspection Using the Digital Image Correlation Method

Aplicação do Método Ransac na Estabilização do Referencial da Câmara em Inspeções de Alta Precisão Utilizando o Método Correlação de Imagens Digitais

Marcio Augusto Reolon Schmidt[1]; Antônio Carlos dos Santos[2]; Jefferson Rodrigo de Souza[3]; Leandro Nogueira Couto[4]; Luciano Oliveira[5]; Dionatan Fabres Carreço[6]

[1] Universidade Federal de Uberlândia. Faculdade de Engenharia Civil. Uberlândia/MG. Brasil. Email: marcio.schmidt@ufu.br
ORCID: https://orcid.org/0000-0003-2716-2360

[2] Universidade Federal de Uberlândia. Faculdade de Engenharia Civil. Uberlândia/MG. Brasil. Email: acds@ufu.br
ORCID: https://orcid.org/0000-0001-9019-4571

[3] Universidade Federal de Uberlândia. Faculdade de Computação Civil. Uberlândia/MG. Brasil. Email: jrsouza@ufu.br
ORCID: https://orcid.org/0000-0001-6422-4722

[4] Universidade Federal de Uberlândia. Faculdade de Computação Civil. Uberlândia/MG. Brasil. Email: leandronc@ufu.br
ORCID: https://orcid.org/0000-0003-2094-1150

[5] Vale S.A. Engenharia de Ferrovias; Vitória/ES. Brasil. Email: oliveira.luciano@vale.com
ORCID: https://orcid.org/0000-0003-0283-4407

[6] Vale S.A. Engenharia de Ferrovias; Vitória/ES. Brasil. Email: dionatan.carreco@vale.com
ORCID: https://orcid.org/ 0009-0002-5442-8320

Abstract: Visual inspection is an important activity for ensuring the safety and efficiency of railway, road, geodetic and geotechnical structures. Very small elements such as cracks can reduce the strength and durability of concrete structures. asphalt pavements and horizontal signage. slopes and more. Conventional assessment methods have limitations in terms of accuracy and quantifying the extent of damage. as they require trained inspection teams. lack regularity in monitoring and are subject to human subjectivity. In this context. the Digital Image Correlation (DIC) method makes it possible to monitor cracks in different types of structures. with impartiality and repeatability. by comparing a reference image taken at the start of monitoring with other images taken periodically. However. there are operational challenges such as maintaining the geometric and positional quality of the reference adopted and its impact on the position and attitude of the sensor over time. This article evaluates the accuracy of inspection images using drones and position injunction with the modified Ransac algorithm for cracks in asphalt and horizontal signs. The results show that the measurements were improved by processing the images and comparing the elements present in the scene.

Keywords: Drone inspection; Ransac estimator; Digital image correlation.

Resumo: A inspeção visual é uma atividade importante para garantir a segurança e a eficiência de estruturas ferroviárias, rodoviárias, estruturas geodésicas e geotécnicas. Elementos muito pequenos como as fissuras podem reduzir a resistência e durabilidade das estruturas de concreto. pavimentos asfálticos e sinalização horizontal. taludes entre outros. Os métodos de avaliação convencionais têm limitações de precisão e quantificação da extensão dos danos. pois exigem equipes de inspeção treinadas. carecem de regularidade no monitoramento e estão sujeitos à subjetividade humana. Neste contexto. o método de Correlação de Imagens Digitais (DIC) permite monitorar fissuras em diferentes tipos de estruturas. com imparcialidade e repetibilidade. comparando uma imagem de referência obtida no início do monitoramento em relação à outras imagens obtidas periodicamente. Entretanto. existem desafios operacionais como a manutenção da qualidade geométrica e posicional da referência adotada e seu impacto na posição e atitude do sensor ao longo do tempo. Este artigo avalia a precisão das imagens de inspeção usando drones e injunções de posição com o algoritmo Ransac modificado para fissuras no asfalto e sinalização horizontal. Os resultados apontam a melhora das medidas por meio do tratamento das imagens. e consequente comparação dos elementos presentes na cena.

Palavras-chave: Inspeção com drones; Estimador Ransac; Correlação de Imagens Digitais.

Received: 25/06/2025; Accepted: 22/10/2025; Publication: 30/10/2025.

1. Introduction

Monitoring activities in various applications such as land use, motorways and railways, as well as isolated structures, have gained prominence in recent years (GROSSO ET AL., 2020; LIANG ET AL., 2023; LAVEZZI ET AL., 2024; LIU ET AL., 2024). In these applications, the use of imaging techniques has gained prominence by allowing monitoring at different scales of acquisition and processing using different platforms. These activities range from medium scales, such as changes in landscape and land use through the growth of anthropized areas (ASLAM et al. 2024; WORACHAIRUNGREUNG et al. 2024), to large scales, such as the monitoring of cracks and faults in asphalt pavements and horizontal signage (AL-DOSARI; HUNAITI; BALACHANDRAN. 2023). to the scale of details such as cracking in concrete, which tends to reduce the effective load (QIAO et al., 2021; ZHANG et al., 2024) and the durability of the material. Therefore, an adequate and periodic monitoring programme is necessary to understand changes in the structural response of elements (LI; YOU; KAEWUNRUEN. 2022; GHERI et al., 2022) and to monitor the expansion and movement of geodetic and geotechnical structures.

These applications share a conventional visual inspection approach to detection (LAI. 2024; MOHAMMED et al., 2020). However, these assessments have limitations in terms of accuracy and ability to systematically quantify the extent and progress of deterioration, as they require time to train the inspection team and lack regularity in monitoring stains and cracks, in addition to being subject to human subjectivity in identification and susceptible to operator fatigue, distractions, and interruptions.

In this context, Digital Image Correlation (DIC) is an alternative technique that allows the measurement of deformations, displacements, and shape changes using optical instruments. According to McCormick and Lord (2010), the DIC technique is more accurate and less subjective than manual measurement methods and allows for a range of applications such as movements, deflections, and deformations of different types of natural or man-made structures. Images can be obtained from a wide variety of sensors, including digital cameras, high-speed video, laser scanning (LAI, 2024), microscopes, including scanning electron microscopes (MCCORMIK; LORD, 2010), and synthetic images, such as radar interferometers and surface roughness images (ZHOU et al., 2021). Measurements made on the images can be correlated with variations in the durability and strength of the monitored elements. To perform DIC, an initial image, corresponding to an undeformed state, is selected as a reference image with which subsequent images will be compared (MOBASHER, 2016). A virtual grid with uniform spacing is used to divide the image into smaller patches, and after deformation, displacements are calculated in relation to each cell of the original grid with the deformed situation to estimate the total deformation field.

One of the most significant challenges in applying the DIC technique is the lack of consistency in the position of the cameras in relation to the object when the method is applied outdoors (in situ). In these cases, i.e. outside the laboratory, the sensor devices are usually incorporated into remotely piloted aircraft (RPA, usually drones or Unmanned Aerial Vehicles (UAVs), temporarily installed on tripods or supports, on robotic inspection vehicles (RIVs) or remotely operated underwater vehicles (ROVs) (Shah et al., 2024). Therefore, with each new survey, the position of the camera sensor and the attitude (rotations and translations of the sensor) of the platform may change relative to previous surveys. Even in RPA systems that use real-time correction technology (GNSS RTK), this position can be altered due to limitations of the positioning system in terms of satellite geometry, signal propagation, and environmental effects, as well as random factors such as natural lighting, clouds, winds, and temporary obstructions such as birds and banners.

However, inspection flights in particular suffer from the propagation of variations in different RPA positions due to environmental conditions, but mainly due to the limitations of the GNSS system itself, even with real-time corrections (RTK). As a result, monitoring by direct image comparison can become biased and inaccurate due to image misalignment and the propagation of variations associated with the coordinates in each image. Figure 1a shows a diagram of images obtained during periodic inspection, and Figure 1b shows the effect of platform translations and rotations when images are superimposed for comparison purposes. It should be noted that for mapping scales, the accuracy using GNSS systems may be sufficient. However, for structural stability and durability inspections, these image mismatches can lead to biased assessments or even make it impossible to monitor movements and cracks in the monitored features.

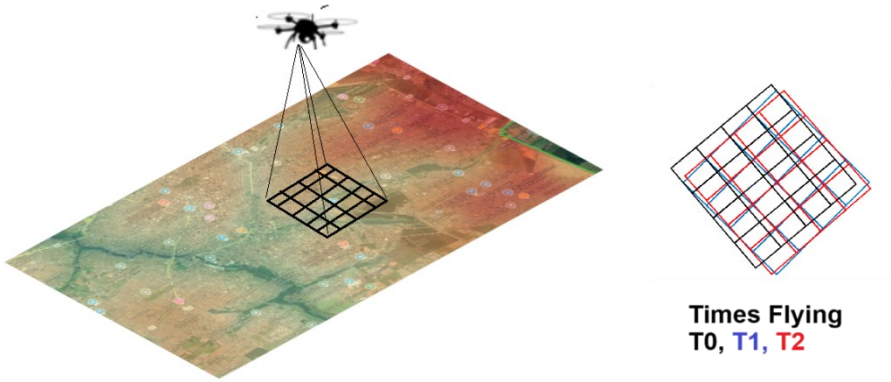

a) b)

Figure 1 - Diagram of changes a) when images were captured and b) effects on the area covered and images captured
Source: Authors

A widely used technique for parameterising residuals and displacements is the Least Squares Method (LSM). This method is applied to solve problems with a redundant system of equations generated from the number of unknowns in the model. This redundancy is caused by determining the coordinates of the same point recorded in different images with partial overlap. Based on the mathematical model, the equations generated with the observations obtained from the images are written in their matrix form as a function of the parameters through the adjustment model (DALMOLIN, 2017). Considering the more general case in which the function is non-linear, the application of least squares requires the linearisation of the system of equations (Equation 3) in the form (DALMOLIN, 2017):

$$X = -(A^T PA)^{-1} \cdot A^T PL \quad (1)$$

The residual vector to be minimised depends on matrix A, which is the matrix of coefficients of the variables defined at the point; observation vectors L and X are the vectors of corrected parameters. However, when the data is not defined in the conventional adjustment, the survey may undergo translation, rotation, and scale change, resulting in the singularity of the normal matrix A and, consequently, making inversion impossible (MAROTTA et al., 2007). In this case, injunctions are used to define points that will serve as control points, which are control pixels in the case of DIC. In general, injunctions involve at least one of the coordinates, direction, and distance. Thus, the injunction matrix would look like in Equation 2:

$$R = \begin{bmatrix} 1 & 0 & 1 & 0 & \dots & 1 & 0 \\ 0 & 1 & 0 & 1 & \dots & 0 & 1 \\ N_1 & -E_1 & N_2 & -E_2 & \dots & N_n & -E_n \\ E_1 & N_1 & E_2 & N_2 & \dots & E_n & N_n \end{bmatrix} \quad (2)$$

In equation 2, N and E are the coordinates in the UTM cartographic projection system and can be expressed in another collected reference. The linearisation of the model with injunctions would be as in Equation 3 (MAROTTA et al., 2007):

$$x = (A^T PA)^+ APL \ (3)$$

Where:
A^T - is the transposed matrix of A
$(A^T PA)^+$ - is the resulting injunction matrix.

Applying constraints to specific pixels is complicated and error-prone, especially in surveys with geographically extensive point clouds and many recorded coordinates. Furthermore, the adjustment presents the challenge of simultaneously estimating correlated variables, which is performed in a high-dimensional search space. This makes optimisation costly and prone to local minima (GUO; GALLEGO, 2024), rendering the method susceptible to outliers and less robust. To solve the problem of outliers, the Ransac algorithm estimates the parameters of a given model from a dataset contaminated by spurious data (outliers), ensuring the minimum number of observations that fit the model (inliers) and eliminating those that differ from the values (outliers) according to non-linear distributions (JANICKA; RAPINSKI, 2014; PÉREZ-SINTICALA et al., 2018). According to Ling et al. (2020), pixels with inliers are usually detected by selecting the minimum number of observations that fit the model and eliminating those that differ from the values (outliers) according to non-linear distributions. 2014; PÉREZ-SINTICALA et al., 2018). According to Ling et al. (2020), pixels with inliers are generally detected by randomly selecting homologous points to determine the orientation parameters and counting the number of inliers whose reprojection errors are at the subpixel level. The process is iterated until the maximum number of inliers is found. In addition to the geometric correspondence between matches and orientation parameters, an alternative way to predict match accuracy is match confidence, which generally reflects the significance of matches when compared to the match results of their surrounding pixels (LING et al., 2020). This article, therefore, proposes that position injunctions can be applied for geometric correction of images between inspections, taking a given pattern as a reference.

Therefore, high-precision monitoring over time requires image position correction to accurately determine the progress of the cracking process, movement, or other sensitive parameters. This article evaluates position injunctions in the parametric method of adjusting observations by least squares estimators, performed by applying the Ransac algorithm, considering a standard image obtained in the first inspection and evaluating the residuals of the positional and scale variations identified in the images. Finally, the estimator is used to realign the other images in relation to the standard image, as occurs in the inspection process performed with drone images.

2. Methodology

Inspection flights were conducted to check horizontal signage on public roads at the Santa Monica campus of the Federal University of Uberlândia (Figure 2), located in Uberlândia, Minas Gerais. The campus covers an area of 280,119 m² and serves a population of 26,270 students and teaching and administrative staff (UFU, 2024). It should be noted that the flights followed the recommendations of the national regulation for RPAs (RBAC-E 94. ANAC. 2017) and that there was no overflight over people in order to ensure operational safety and ethical aspects of the research

.

Figure 2 - Identification of the test area on the Santa Monica campus of UFU
Source: UFU (2024)

A Phantom 4 RTK drone was used to conduct the surveys. This equipment has a 1" CMOS sensor capable of recording 4K videos at 60 fps and photos with a resolution of 20 Mp. This model has a GPS/GLONASS positioning system with an

integrated RTK module for real-time corrections of positioning data, ensuring centimetre accuracy for real-time surveys. It records satellite observation data for sub-centimetre accuracy applications using Post-Processed Kinetics (PPK) (DJI. 2024). Table 1 shows the model specifications.

Table 1 - Specifications of the remotely piloted aircraft used

ARP parameters	
Attributes	**Specifications**
Brand	DJI
Model	Phantom 4 RTK
Take-off weight	1391g
Max. flight time	30 min
Max. flight distance	Up to 5 km (CE transmission standard)
Max. flight speed	50 kph (P-mode) ou 58 kph (A-mode)
Operating temperature	0° to 40°C
Operating frequencies	2.400 GHz to 2.483 GHz
GNSS	GPS+GLONASS+GALILEO
Hover accuracy Range	0.1m (H e V) with RTK, 0.1m (V) and 0.5m(H) with GNSS only
Sensor	CMOS of 1”
Effective resolution	20 Mp
Aperture	f 2.8 a f 11
Image size	4864 x 3648 (4:3)
Stabilisation	Triaxial (tilt, roll, and yaw)

Source: DJI (URL 1)

Eight flight tests were conducted with flight height variations of 20 m and 30 m, configured with 40% lateral coverage, 70% longitudinal coverage, and flight speeds according to the Drone Harmony mobile software planning. These flights were conducted on different days between 20 and 26 February 2025 to ensure variability in GNSS signals and wind conditions, ambient lighting, and other interference to approximate actual survey conditions. The software used for processing was Pixel4Dmapper from Pix4D. The collection plan considered the use of two control points obtained with an AshTec single-frequency receiver (L1 carrier) with a recording interval of 5 seconds and a baseline for the reference station less than 100 m from the RBMC MGUB station. The use of control points helps to minimise the dome effect (curvature of flight lines that generates a convex curvature effect in relation to the reference plane). Cracks in the asphalt, horizontal signage and other elements in front of building 1Y on the UFU campus in Santa Monica were used as identification objects.

In this study, the DIC technique was applied considering the reference grid as the pixel of the images itself, since there is no significant deformation due to perspective effects, but only displacements and rotations of the sensor set reference frame. Understanding the images from the first survey of each area as the initial instant (t0), as fixed images, and the other images compared to this reference, understood as images to be adjusted, the displacements were evaluated by tracking the centroid of the pixels in the reference image and their counterparts in the subsequent images. Although this approach presents a disadvantage in the edge areas of the adjusted images, the evaluation area is preserved and it is possible to correlate the identified points.

A script developed in Matlab was used for image correlation and analysis. The steps in the process include using the camera calibration parameters such as effective image size. central pixel coordinates and calibrated focal length obtained in Pix4D processing; conversion of images to monochrome with automatic threshold contrast correction; application of SURF (Speeded up Robust Feature) detection; and identification of pairs of homologous points from thresholding. The SURF detector is superior to the Harris filter (HARRIS; STEPHENS. 1988) in terms of the number of recognisable points (KUCAK et al., 2020). While Harris uses thresholds and edge hysteresis calculated from the conversion of images to binary, Surf identifies blobs, i.e. areas of intensity in the processed images as a way to select homologous vertices and index the pixels in pairs. Compared to other methods such as SIFT and ORB, the SURF estimator stands out for its efficiency in processing points, which makes it efficient in images at different scales. This detector uses box filters on the entire image and wavelet-based descriptors, which speeds up processing and makes it efficient with images at different scales and ensures invariance to rotation and contrast (KARAMI, PRASADA AND SHEHATA, 2015; BENEVIDES et al., 2022). The SIFT method is an effective and efficient detector for geometric aspects of images, but it faces high

computational costs, while the ORB method uses the FAST detector associated with the BRIEF descriptor, which incurs less robustness in processing (KARAMI, PRASADA, AND SHEHATA; 2015).

Once the pixels have been identified and indexed, the matrix of validated pairs takes on the Mx3 format, considering their coordinates and associated intensities. In this study, the fundamental matrix was constructed from the pairs of homologous points validated in the previous steps. This matrix was chosen because the images were collected by the same sensor set on different dates. The use of the essential matrix was not possible because the camera was not absolutely calibrated and, due to issues with the drone's position, it was assumed that the points in the scene in the test area were not coplanar, which makes homography unfeasible.

The estimation of the fundamental matrix parameters was performed using the MSAC method (YANG et al., 2014; AKDIM et al., 2025). The MSAC (Modified Ransac) estimator generally converges faster than Ransac and has the characteristic of avoiding local minima (ZHANG; SHI; XU, 2019) by updating the index at each interaction, considering Sampson's distance. This convergence may be influenced by the characteristics of the images, such as the number of details, and therefore it may be necessary to vary the number of iterations required to define the matrix.

The number of iterations was set at 2000 after evaluating the results considering a variation starting at 500, 1000, 2000, and 3000. Finally, the geometric transformation between the images was calculated using a projective model, applied to the inliers selected by MSAC under a threshold of 0.95 and random seeds for each test. This transformation allows for compensation of the relative displacements between the image capture positions and the perspective distortions caused by the platform's attitude on different dates.

For positional evaluation, in addition to the overlap and linear measurement between points, the calculation of root mean square errors (RMSE) in relation to GNSS RTK (ground control point – GCP) surveys was used, as in Jiménez-Jiménez et al. (2021) and Guimarães et al. (2025), presented in equations 6. 7 and 8, and the quality verified with a 95% confidence interval and bootstrap with 1000 samples.

$$RMSE_x = \sqrt{\frac{\sum_{i=1}^{n}(x_i - x_r)^2}{n-1}} \quad (6)$$

$$RMSE_y = \sqrt{\frac{\sum_{i=1}^{n}(y_i - y_r)^2}{n-1}} \quad (7)$$

$$RMSE_r = \sqrt{RMSE_x^2 + RMSE_y^2} \quad (8)$$

3. Results and discussions

The calibration results are presented in Table 2 below. A focal length of 8,776 mm was identified in the Phantom 4 drone sensor system.

Table 2 – Calibration parameters obtained

Calibration parameters

Parameters	Focal distance (f) (mm)	Centre X (mm)	Centre Y (mm)	R1	R2	R3	T1	T2
Inicial Values	8.600	5.676	4.306	-0.270	0.112	-0.032	0.000	-0.001
Calibrated Values	8.776	5.686	4.261	-0.012	-0.005	0.013	-0.001	-0.000

Uncertainties (Sigma)	0.013	0.000	0.001	0.000	0.001	0.001	0.000	0.000

Source: Authors

A set of images extracted from two areas of the campus from the flights performed and classified according to flight height was selected. The images from the first flight at each height, 20 m and 30 m, respectively, were used as standard data. They were designated as fixed, as they were considered the first inspection flight in each situation. The images from subsequent flights were named as mov, followed by the flight number (mov 01, mov 02, and mov 03). The developed script performed an automated search for homologous pairs of the surf filter, which considers the position and spectral response of the pixels to perform the correlation in a list of indexed pairs. The average number of correlated pixels was 137 for each set of images (fixed, mov). As a verification step, the homologous points were identified and correlated using lines for visual comparison (Figure 3) with the identification of internal points and the elimination of pairs considered external points.

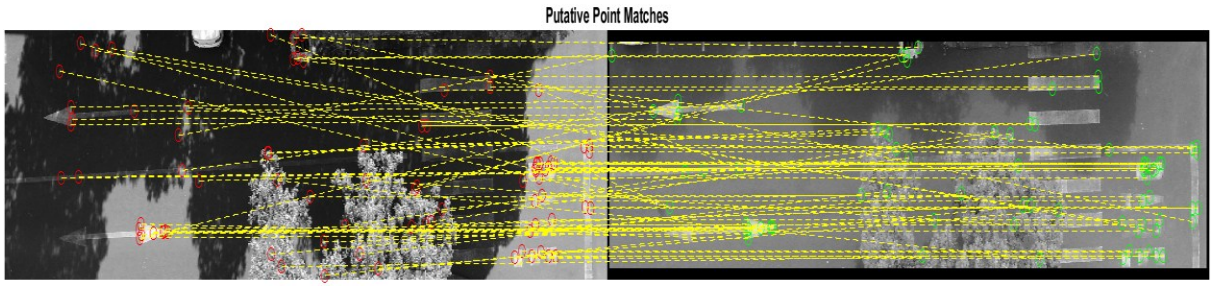

Figure 3 – Indication of identified homologous points
Source: Authors

The Ransac method was also compared to the parametric MMQ. The number of iterations was varied to 500, 1000, 2000, and 3000. These iterations vary according to the computational effort required to evaluate and solve the matrices, eliminating outliers. A smaller number of iterations, in the range of 500 and 1000, presented problems of non-convergence of the system of equations or problems of inversion of the characteristic matrix. Although none of the tests reached the threshold of 0.95, the highest values of inliers were achieved, for the most part, with 2000 iterations. The inlier values ranged from 0.471 for the 20m flight with 500 iterations to 0.825 for the same flight with 2000 iterations. The other images ranged from above 0.584 to close to the maximum value identified. Comparatively, MMQ presented results that were systematically lower than Ransac, even with variations in the number of interactions.

However, the most relevant term for estimating the matrices was the number of homologous pairs detected. In the different checks carried out, the number of 60 pairs of homologous pixels suggests to be the threshold for the most effective results. Although the average was 137 pairs, three images with more significant relative displacements in relation to the control images reached only 27, 29, and 53 homologous pairs, and the results were images with less adherence to the control image, which would make it impossible to use them for monitoring. This also implies that a small image coverage area or images with little detail may suffer from inadequate scaling of the coefficient matrix (A), and their inversion may be impaired, requiring the use of the pseudo-inverse matrix. Figure 4a shows, for example, the combination of image mov 3 on the first flight at a height of 20 m, and Figure 4b shows image mov 2 on the 30 m flight. In this figure, some of the identified homologous pairs are shown in the superimposed images. The still images (standard images) are highlighted in cyan and the moving images are in magenta (Figure 4).

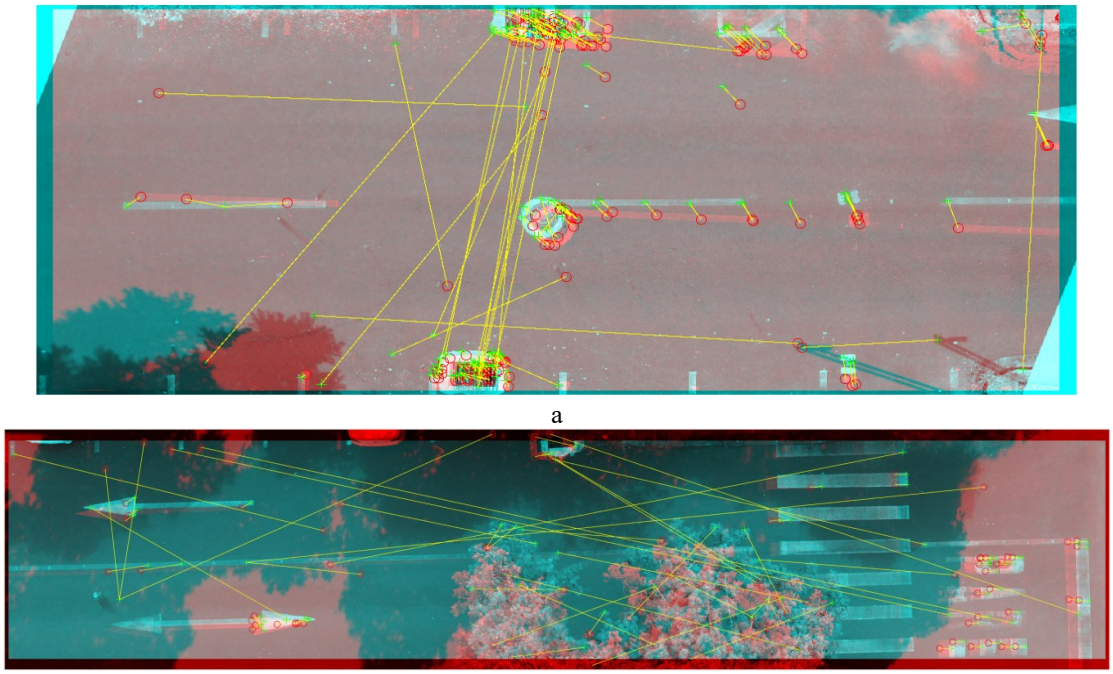

Figure 4 - Identification of homologous pairs in the moving and reference images a) mov3 at a height of 20m. and b) mov2 at a height of 30m.
Source: Authors

The fundamental translation and rotation matrix of each moving image relative to the standard (fixed) image was estimated from the validated points. Table 3 shows the translation and rotation results of each moving image relative to its fixed images in pixels using the Ransac method.

Table 3 - Ransac image adjustment results

Matrix results using the MSAC method							
		Translation (in pixels)			**Rotation (dimensionless)**		
Flying height of 20 metres							
		X	Y	Z			
AREA 1	MOV01	0.9887	0.1495	0.0068	0.9480	0.2794	0.1522
					0.1995	-0.1496	-0.9684
					-0.2478	0.9484	-0.1976
	MOV 02	-0.9989	-0.0465	-0.0016	-0.9363	0.3495	0.0357
					0.1012	0.3656	-0.9253
					-0.3364	-0.8627	-0.3776
	MOV 03	-0.9994	-0.0357	0.0034	-0.9825	0.1822	0.0383
					-0.0503	-0.0619	-0.9968
					-0.1792	-0.9813	0.0700
AREA 2	MOV01	0.9959	0.0906	-0.0047	0.8447	-0.5283	0.0853
					0.0801	-0.0327	-0.9962
					0.5292	0.8484	0.0147

	MOV 02	0.9443	-0.3290	-0.0034	0.8901	-0.3137	-0.3305
					-0.3484	-0.0009	-0.9373
					0.2937	0.9495	-0.1101
	MOV 03	-0.9480	0.3184	0.0052	0.92321	0.2220	0.3137
					-0.3065	-0.0669	0.9495
					0.2318	-0.9728	0.0063
Flying height of 30 metres							
		X	Y	Z			
AREA 1	MOV01	-0.9361	-0.3517	0.0037	0.5414	0.3594	0.7601
					0.7645	-0.5867	-0.2671
					0.3500	0.7257	-0.5924
	MOV 02	-0.9729	0.2310	0.0049	0.9590	-0.1705	0.2263
					-0.2236	0.0355	0.9740
					-0.1742	-0.9847	-0.0041
	MOV 03	0.9961	0.0886	0.0012	0.9904	0.1059	0.0894
					0.0808	0.0828	-0.9933
					-0.1126	0.9909	0.0735
AREA 2	MOV01	-0.9080	0.4188	0.0041	-0.9004	0.1320	-0.4146
					0.4108	-0.0559	-0.9100
					-0.1433	-0.9897	-0.0039
	MOV 02	-0.9454	0.3259	0.0056	0.8808	-0.3428	-0.3266
					-0.3700	-0.0682	-0.9265
					0.2953	0.9369	-0.1869
	MOV 03	0.9381	-0.3464	-0.0054	0.8306	-0.4428	0.3378
					-0.3604	0.0352	0.9321
					-0.4246	-0.8959	-0.1304

Source: Authors

Regarding geometric accuracy, these values can be multiplied by the GSD (ground sampling distance) of each flight obtained through complete processing of the survey blocks. For the 20 m flights, the average GSD value was 0.537 ± 0.013 cm/pixel, and the 30 m flights had an average GSD value of 0.7983 ± 0.026 cm/pixel.

Table 4 shows the absolute mean of the displacements and the mean of the absolute values, which is a measure that calculates the dispersion of the data and helps to identify outliers. The mean displacement values were calculated using the flat Euclidean distance of 5.36 mm and 7.94 mm for the 20 m and 30 m flights.

Table 4 - Average deviations between reference and mobile images after processing

		Metres		
		X	Y	Z
20m	Mean	0.0053	0.0009	0.0000
	Deviation	0.0001	0.0007	0.0000
30m	Mean	0.0076	0.0023	0.0000
	Deviation	0.0002	0.0009	0.0000

Source: Authors

The results of the adjustment and registration after applying the MSAC method can be seen in detail in Figure 5. In Figures 5a and 5b, 20 m flight, and in Figures 5c and 5d, 30 m flight, the details show cutouts made in areas where images

overlap, i.e., areas near the edge where images complement each other in the mosaic of stacked images. It is possible to see the continuity of the characteristics, so that the measurement can be performed with the same reference set for the images from the first flights. The deviations, as shown in Table 3, are less than 7 pixels between images. The RMSE was calculated for the East component and for the North component separately and then the overall RMSE using formulas 6.7 and 8, reaching RMSE values of 0.979 pixels and 0.949 pixels for the 20 m and 30 m flights, respectively. RMSEy values of 0.202 pixels and 0.313 pixels for 20m and 30m and a total RMSE of 0.999 pixels for both cases. These values indicate that the x component had greater deviations in the surveys carried out and may indicate a trend in the system for the region.

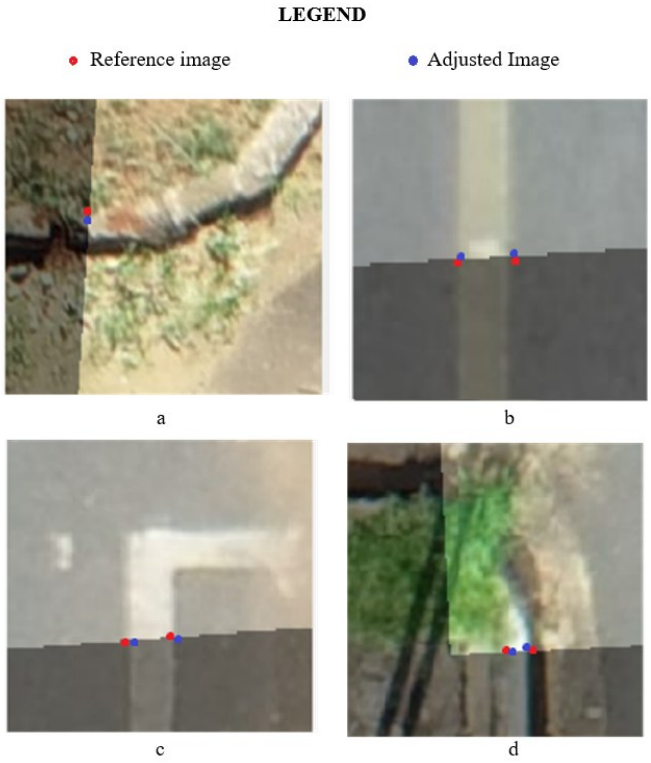

Figure 5: Details of the corrected and superimposed images after the Ransac method: a) and b) mov03 at a height of 20 m. c) and d) mov03 at a height of 30 m.
Source: Authors

Finally, a significance analysis of the reprojection errors was generated for each of the image sets analysed. The criteria of average reprojection error, standard deviation of error, maximum reprojection error, and RMSE of reprojection based on the inlier values were analysed. The flights performed at a height of 30 m presented the lowest values in the error analysis, with the last day (4th flight) presenting an average reprojection error of 0.8804 pixels, standard deviation of error of 0.9119 pixels, maximum reprojection error: 4.2944 pixels, and reprojection RMSE: 1.2593 pixels. The same analysis for flights at a height of 20 m obtained higher values, with the analysis for the same day (4th flight) showing an average reprojection error of 108.3382 pixels, standard deviation of error of 418.6456 pixels, maximum reprojection error of 1839.9949 pixels, and reprojection RMSE: 425.8492 pixels. Considering the values found, these results may indicate that flight height may be a factor of greater relevance in reprojection quality.

4. Final considerations

Environmental factors and the characteristics of the GNSS system can influence the extraction of geometric information from images obtained at different monitoring periods and degrade the accuracy of measurements in images over time. In this case, measurement accuracy is an essential parameter for correlation with aspects of durability and resistance of the analysed elements. These differences, even when using the same flight plans and care in platform configuration, can make it impossible to directly compare images in an automated inspection process.

In this context, the application of the MSAC estimator approach to filter and register images proved to be a fundamental quality control method to reduce distortions in the sensor position when taking photographs at different times. Image processing and correction proved to be an important tool for correcting images and monitoring cracks, horizontal signage, and other characteristics of the study area. The survey flights achieved an accuracy compatible with topographic mapping activities. However, the application of the DIC method as a large-scale inspection tool requires the correction of the perspective centre of the images obtained in different field campaigns in order to measure and monitor them before correlating them with the physical and durability properties of the inspected elements.

Alternatively, the results indicate that the sensor position should be fixed whenever possible, or that the optical system of the sensor devices should be sufficiently close to the target so that displacements become insignificant on the survey scale. This shows that the monitoring scale is influenced by the platform used and that, for greater accuracy, it is necessary to reduce the degrees of freedom of the sensor devices in terms of displacement and attitude. Future work could include determining the minimum flight height to increase the accuracy of drones and the distance for sensors supported on tripods or other types of support, as well as repeating the study in other areas with different characteristics, such as more urbanised environments.

Acknowledgements

The authors would like to thank the Federal University of Uberlândia and to Vale S.A. for its support and funding of this research, which is associated with patent application number BR-1020250026880, dated 11/02/2025.

References

Akdim. K.; Roukhe. H.; Roukhe. A. Image Registration using Median Absolute Deviation –based Adaptive RANSAC. *Engineering. Technology & Applied Science Research*. n.15. v. 3. 22378–22387. 2025. https://doi.org/10.48084/etasr.10121.

AL-Dosari K.; Hunaiti Z.; Balachandran W. Systematic Review on Civilian Drones in Safety and Security Applications. *Drones*. v.3. n.7. 2023. https://doi.org/10.3390/drones7030210

Aslam. R.W.; Shu.H.; Tariq.A.; Naz.I.; Ahmad. M. N.; Quddoos. A. Javid. K.; Mustafa. F.; Aeman. H. Monitoring landuse change in Uchhali and Khabeki wetland lakes.Pakistan using remote sensing data. *Gondwana Research*. n. 129. 2024. https://doi.org/10.1016/j.gr.2023.12.015g

Benevides. R. A.L.; Pitombeira. K.; Centeno. J.; Simões. P. R. Automatic. accurate and robust image registration with adapted RANSAC (Random Sample Consensus) for SIFT (Scale Invariant Feature Transform) descriptor. (2022). Research. Society and Development. 11(14). e383111436631. https://doi.org/10.33448/rsd-v11i14.36631

Dalmolin. Q. Algumas Considerações Sobre a Avaliação Do Resultado De Um Ajustamento De Observações. *Revista Brasileira de Cartografia.* n. 69. v.3. 533-539. 2017. Sociedade Brasileira de Cartografia. Geodésia. Fotogrametria e Sensoriamento Remoto. ISSN: 1808-0936

DJI. Phantom 4 RTK - Specifications. Avaiable at: https://www.dji.com/br/phantom-4-rtk/info. Accessed in: 03/04/2025.

Gehri. N.; Mata-Falcon. J.; Kaufmann. W. Refined extraction of crack characteristics in large-scale concrete experiments based on digital image correlation. *Engineering Structures.* n 251. 2022.h https://doi.org/10.1016/j.engstruct.2021.113486

Grosso. R.; Mecca. U.; Moglia. G.; Prizzon. F.; Rebaudengo. M. Collecting Built Environment Information Using UAVs: Time and Applicability in Building Inspection Activities. Sustainability. 12(11). 2020.

https://doi.org/10.3390/su12114731

Guimarães. M.J.M; Santos. A. C. da S.; da Silva. A.S. Ribeiro. R.P.; Barros. J.R.A.; Lopes. I. Mapeamento topográfico com aeronave remotamente pilotada para fins de georreferenciamento de propriedades rurais. *Revista de Geociências do Nordeste*. v. 11. nº 1. 2025. https://doi.org/10.21680/2447-3359.2025v11n1ID34481

Guo. S.; Gallego. G. Event-based Photometric Bundle Adjustment. *Computer Vision and Pattern Recognition*. 2024. https://doi.org/10.48550/arXiv.2412.14111

Harris. C.; M. Stephens. A Combined Corner and Edge Detector. *Proceedings of the 4th Alvey Vision Conference*. pp. 147-151. 1988. Avaiableat:https://citeseerx.ist.psu.edu/document?repid=rep1&type=pdf&doi=88cdfbeb78058e0eb2613e79d1818c567f0920e2

Jiménez-Jiménez. Sergio Iván. Waldo Ojeda-Bustamante. Mariana de Jesús Marcial-Pablo. and Juan Enciso. Digital Terrain Models Generated with Low-Cost UAV Photogrammetry: Methodology and Accuracy. *ISPRS International Journal of Geo-Information.* v. 10. n. 5. 2021. https://doi.org/10.3390/ijgi10050285

Janicka. J.; Rapinski. J. Outliers detection by Ransac algorithm in the transformation of 2d coordinate frames. *Boletim de Ciências Geodésicas*. v. 3. n.20. 2014. ISSN 1982-2170 https://doi.org/10.1590/S1982-21702014000300035

Kucak A.; Yakar I.; Bilgi S.; Erol S.; Dervisoglu A. A Comparative Analysis of Speeded Up Robust Features (SURF) and Harris Algorithms in Point Cloud Generation. Proceedings 1st Intercontinental Geoinformation Days (IGD). 2020. Turquia

Karami. E.; Prasad. S.; Shehata. M. Image Matching Using SIFT. SURF. BRIEF and ORB: Performance Comparison for Distorted Images. Proceedings: 2015 Newfoundland Electrical and Computer Engineering Conference. Canada. https://doi.org/10.48550/arXiv.1710.02726.

Lai. M. 2024. A study on drone-based detection and recognition of concrete surface cracks in tunnels using advanced imaging and machine learning techniques. *Advances in Operation Research and Production Management*.v. 3. 2024. https://doi.org/10.54254/3029-0880/2024.19215

Lavezzi. G.; Ciarcià. M.; Won. K.; Tazarv. M. A DIC-UAV based displacement measurement technique for bridge field testing. Engineering Structures. Volume 308. 2024. ISSN 0141-0296. https://doi.org/10.1016/j.engstruct.2024.117951.

Li. D.; You. R.; Kaewunruen. S. Crack Propagation Assessment of Time-Dependent Concrete Degradation of Prestressed Concrete Sleepers. Sustainability. n. 14. 2022. https://doi.org/10.3390/su14063217

Liang. H.; Lee. S.-C.; Bae. W.; Kim. J.; Seo. S. Towards UAVs in Construction: Advancements. Challenges. and Future Directions for Monitoring and Inspection. *Drones*. 7(3). 2023. https://doi.org/10.3390/drones7030202

Ling. X.; Huang. X.; Zhang. Y. e Zhou. G. Matching Confidence Constrained Bundle Adjustment for Multi-View High-Resolution Satellite Images. *Remote Sens*. v.20. n.12. 2020. https://doi.org/10.3390/rs12010020

Liu. B.; Yang. T.; Wu. X.; Wang. B.; Zhang. H.; Wu. Y. UAV imagery-based railroad station building inspection using hybrid learning architecture. Measurement Science and Technology. 35. 2024. http://dx.doi.org/10.1088/1361-6501/ad4ab5.

Liu. G.; Luo. J.; Yang. Q.; Law. S.; He. C. Non-contact Structural Displacement Measurement using UAV and DIC with Non-coplanar Fixed Region of Interest. Measurement. Volume 242. Part B. 2025. ISSN 0263-2241. https://doi.org/10.1016/j.measurement.2024.115936.

Marotta. G.S.; Silva. A.S.; Gonçalves. R. P.; Andrade. R. J. DE O.; Assis. L. C. de. Estimativa da precisão posicional utilizando ajustamento de observações clássico e livre. *Proceedings: XXIII Congresso Brasileiro de Cartografia*. Rio de Janeiro. Brasil. 2007. https://doi.org/10.13140/2.1.3048.2884

McCormick. N.; Lord. J. Digital Image Correlation. *Materials Today*. v.13. n.12. 2010. ISSN 1369-7021. https://doi.org/10.1016/S1369-7021(10)70235-2.

Mobasher. Textile fiber composites: Testing and mechanical behaviour. Textile Fibre Composites in Civil Engineering. Editor(s): Thanasis Triantafillou. Woodhead Publishing. 2016. Pages 101-150. ISBN 9781782424468. https://doi.org/10.1016/B978-1-78242-446-8.00006-9.

Mohammed.Y.;Uddin. N.; Tan. C. SHI. Z. Crack Detection using Faster R-CNN and Point Feature Matching. *Civil Enginnering Research Journal*. v. 10. n.3. 2020. https://doi.org/10.19080/CERJ.2020.10.555790

Pérez-Sinticala. C.; Janvier. R.; Brunetaud. X.; Treuillet. S.; Aguilar. R.; E Castañeda. B. Evaluation of Primitive Extraction Methods from Point Clouds of Cultural Heritage Buildings: An Interdisciplinary Approach. In: Aguilar. R.; Torrealva. D.; Moreira. S.; Pando. M. A.; Ramos. L. F. (eds) Structural Analysis of Historical Constructions. RILEM Bookseries. v. 18. Springer. Cham. https://doi.org/10.1007/978-3-319-99441-3_250

Qiao. W.; Zhang. H.; Zhu. F.; Wu, Q. A Crack Identification Method for Concrete Structures Using Improved U-Net Convolutional Neural Networks. *Mathematical Problems in Engineering*. 2021. Wiley Online Library. https://doi.org/10.1155/2021/6654996

Shah. F.M.; Shah.Z. M.; Janjua. G.; Zhang. Y. X. Crack Detection on Civil Structure Using Efficient Image Processing and Computer Vision Approach. *Proceedings: Advances in Science and Engineering Technology International Conferences (ASET)*. 2024. https://doi.org/10.1109/ASET60340.2024.10708670

UFU. Universidade Federal de Uberlândia. Pró-reitoria de Planejamento. *Anuário 2023*. Avaiable at: https://proplad.ufu.br/central-de-conteudos/documentos/2024/06/anuario-2023

Zhang. T.; Qin. L.; Zou. Q.; Zhang. L.; Wang. R.; E Zhang. H. 2024. CrackScopeNet: A Lightweight Neural Network for Rapid Cracks Detection on Resource-Constrained Drone Platforms. *Drones*. v.9. n.8. 2024. https://doi.org/10.3390/drones8090417

Zhang. Q.; Shi. B.; e Xu. H. Least Squares Consensus for Matching Local Features. *Information*. n. 10. 2019. https://doi.org/10.3390/info10090275

Zhou. K.; Lei. D.; He. J.; Zhang. P.; Bai. P.; E Zhu. F. Single micro-damage identification and evaluation in concrete using digital image correlation technology and wavelet analysis. *Construction and Building Materials*. v. 267. 2021. https://doi.org/10.1016/j.conbuildmat.2020.120951

Wang, Y.; Huang, H.; Dong, Z.; Wu, M. Modified RANSAC for Sift-Based InSAR Image Registration. *Progress In Electromagnetics Research.* v. 37. 2014. https://doi.org/10.2528/PIERM14042202

Worachairungreung.M.; Kulpanich.N.; Thanakunwutthirot. N.; Hemwan. P. Monitoring Agricultural Land Loss by Analyzing Changes in Land Use and Land Cover. *Emerging Science Journal.* v.8. n.2. 2024. http://dx.doi.org/10.28991/ESJ-2024-08-02-020